Pap-smear image classification by using a fusion of texture features

André Ricardo Backes*
*School of Computer Science, Federal University of Uberlândia
Av. João Naves de Ávila, 2121, 38408-100 Uberlândia, MG, Brazil
Email: *arbackes@yahoo.com.br*

***Abstract*—In this paper we address the problem of *pap-smear* image classification. These images have great medical importance to diagnose and prevent uterine cervix cancer and have been intensively studied in computer vision research. We evaluated 19 texture features on their ability to discriminate between two classes (normal and abnormal) of *pap-smear* images. We performed the classification of these feature using three different approaches: K-Nearest Neighbors (KNN), Support Vector Machine (SVM) and Linear Discriminant Data (LDA). We conducted this evaluation considering each texture method independently and their concatenation with others. Results show combining methods improves the accuracy, surpassing most of the compared methods, including some deep learning approaches.**

I. Introduction

One of the main branches of computer vision research is the medical image analysis area, which, among other goals, aims to increase the diagnosis accuracy, speed up the analysis process, and provide a second opinion to the human specialists. Over the last years, this research area has continually gained powerful computational approaches to analyze images from a great variety of human tissues. To cite some recent instances, paper [1] proposes automatic detection of lung nodules using deep convolutional neural networks. [2] classifies breast biopsy images using deep learning models. In [3] authors propose a cascade-learning approach to segment tumor epithelium. We evaluated the approach's performance in colorectal cancer.

Among the relevant attributes to exploit in medical image analysis, texture is surely one of the most relevant. It is easily understood by humans, but it is hard to establish to it a unique definition. Paper [4], for example, defines a texture image as an arrangement of sub-patterns, which can be pixels, regions or visual attributes (many images of man-made objects fall within this description, such as walls, roofs, fabrics with repetitive patterns etc.). However, such definition does not encompass the stochastic patterns present in natural textures (for instance, images of smoke, dust etc.). For such images, paper [5] describes them as having "random but persistent patterns", which "result in a cloud-like texture appearance".

Throughout the years, many methods have been developed to analyze textures. According to [6], these methods can be grouped into seven categories: Statistical (co-occurrence matrices [7], Weber local descriptors [8] etc.); Structural; Transform-based (Fourier descriptors [9] and Gabor filters [10], for instance); Model-based (methods based on complex networks [11], fractal dimension [12] etc.); Graph-based (shortest paths in graphs [13], [14], for instance); Learning-based (grounded on neural networks [15]–[17] and vocabulary [18]); and Entropy-based.

In this work, we evaluate 19 texture features to the problem of *pap-smear* images classification. These images are commonly used to diagnose and prevent uterine cervix cancer. Because of such medical importance, this type of image has been intensively studied in computer vision research. Given a dataset of *pap-smear* images, we computed the texture features for each method. We must emphasize that the number of descriptors varies from method to method. We used three different approaches to classify the features: K-Nearest Neighbors (KNN), Support Vector Machine (SVM) and Linear Discriminant Data (LDA). Additionally, we evaluated the discrimination power of each texture method independently and when combined with other texture methods.

We organized the remaining paper as follows: Section II discusses the literature focused on *pap-smear* images classification. Section III presents details of the dataset, and describes the texture analysis and classifiers used during the experiments. Section IV presents and discusses our results while Section V presents our concluding remarks.

II. Related Work

Because of its medical importance, *pap-smear* images have been intensively studied in computer vision research as described as follows.

In paper [19], the authors propose a method to segment nuclei of cervical cells and to classify them based on shape and texture features. The paper [20] presents a multi-pass watershed-based approach to segment nucleus and cytoplasm from overlapping cervical cell images. In [21], the work introduces an automatic method for segmenting cervical nuclei using convolutional neural network and connected random field.

The authors in [22] use shape, texture and color features to classify the cervical dysplasia into two-level (normal and abnormal). They obtain the classification of the samples by using an ensemble method, which integrates the decision of three classifiers. In [23], the authors proposed a modification of the local binary patterns (LBP) method to classify *pap-smear*

978-1-6654-5385-1/22/$31.00 ©2021 IEEE

images. Instead of using a fixed radius, the authors proposed an adaptive neighborhood radius for each pixel and a spatial adjacent histogram strategy to encode the micro-structures for image representation.

Authors in [24]. present a bag-of-words (BoW) approach for microscopic image classification. They used the locality-constrained linear coding for local feature encoding instead of vector quantization and a softmax regression as a classifier. In [25], the authors used transfer learning and concatenated the features from three Convolutional Neural Networks (Inception-v3, Resnet152 and Inception-Resnet-v2). They used these features to train two fully-connected layers to perform classification.

III. Materials and Methods

A. Dataset

The pap-smear database [26] is composed of 917 cell images unevenly divided into seven classes. They are (with the respective number of samples): Superficial squamous epithelial (74), Intermediate squamous epithelial (70), Columnar epithelial (98), Mild squamous non-keratinizing dysplasia (182), Moderate squamous non-keratinizing dysplasia (146), Severe squamous non-keratinizing dysplasia (197) and Squamous cell carcinoma in situ intermediate (150). The first three classes are considered "normal" (242), and the last four classes are considered "abnormal" (675). Figure 1 shows one cell sample of each class. This work focuses only on the two-class problem.

B. Texture Analysis Methods

For this work we selected 19 texture features based on their good results reported in the literature, as also their wide range of applications and novelty. We describe each method as follows:

- First-order: we computed 5 descriptors (mean, variance, kurtosis, energy and entropy) from the image histogram;
- Haralick [27]: this method describes the texture image using the joint probability distributions between pairs of pixels at a given distance and direction. We used non-symmetric matrices with $\theta = \{0°, 45°, 90°, 135°\}$ and distances $d = \{1, 2\}$. From each matrix we computed energy and entropy, totaling 16 descriptors;
- Fourier descriptors [9]: this method uses the bi-dimensional Fourier transform and the *shifting* operator over the resulting spectrum to compute spectrum descriptors. In this work we computed 15 descriptors, each one representing the sum of all absolute coefficients at the same radial distance from the center of the image;
- Wavelet descriptors [28], [29]: given a texture image, we used Daubechies 4 to compute three dyadic decomposition. We computed energy and entropy from horizontal, vertical and diagonal detail coefficients of each decomposition, totaling 18 descriptors;
- Gray Level Dependence Matrix (GLDM) [30]: it uses the frequency of occurrence of two pixels with a determined absolute difference in intensity given a specific distance and intersample space. We computed the descriptor using four distances ($(0, d)$,$(-d, d)$,$(d, 0)$, and $(-d, -d)$) and three intersample spaces (1, 2 and 5). We computed five measurements (contrast, angular second moment, entropy, mean, and inverse difference moment) from each probability-density function, totaling 60 descriptors;
- Discrete Cosine Transform (DCT) [31]: we used three 1D DCT basis vectors ($U_1 = [1, 1, 1]^T$, $U_2 = [1, 0, -1]^T$, and $U_3 = [1, -2, 1]^T$) to compute eight 3×3 DCT masks. We applied each mask to the input texture image and computed the local variance of the output, totaling 8 descriptors;
- Local Binary Patterns (LBP) [32]: this method describes a texture based on histograms of local binary patterns related to the spatial configuration of local features of an image. We evaluated three different configurations, $(P, R) = \{(8, 1), (16, 2), (24, 3)\}$, thus leading to three histograms;
- Lacunarity [33]: this method measures the spatial dispersion of gaps of a specific size in order to describe a texture image. We used the gliding-box approach and two threshold methods (local and global) to compute the gaps. The number of box sizes was defined to maximize the accuracy;
- Lacunarity 3D [33]: this method considers the gray level intensity as a third dimension of the image and it uses the gliding-box approach to measure the number of gaps in a 3D grid. The number of box sizes was defined to maximize the accuracy;
- Differential lacunarity [34]: this method considers the local difference between minimum and maximum gray levels and the gliding-box approach to measure the number of gaps in a texture image. The number of box sizes was defined to maximize the accuracy;
- Fractal Descriptors from Local Binary Patterns (LBP+FD) [35]: this method uses LBP to compute image patterns and the Bouligand-Minkowski fractal dimension to extract meaningful information from these patterns. We computed eight fractal dimension values from each LBP pattern ($N = 11$), totaling 80 descriptors;
- Randomized Neural Network (RNN) descriptors [16]: this method trains an RNN using local texture patterns. Then, it uses the weights of the output neuron layer as features to describe the input texture image. We used the rotation invariance approach, totaling 30 descriptors;
- Tourist Walk [36]: this method uses a deterministic rule to explore the image content, thus moving a tourist walker from pixel to pixel in the image. We considered the specification described in [36], totaling 48 descriptors;
- Fractal Descriptors: we used the log-log curve computed from the a fractal dimension method as descriptors to characterize a texture pattern in terms of its complexity. We evaluated three approaches to compute the log-log curve: Bouligand-Minkowski [37], mass-radius [38] and average square difference [39].

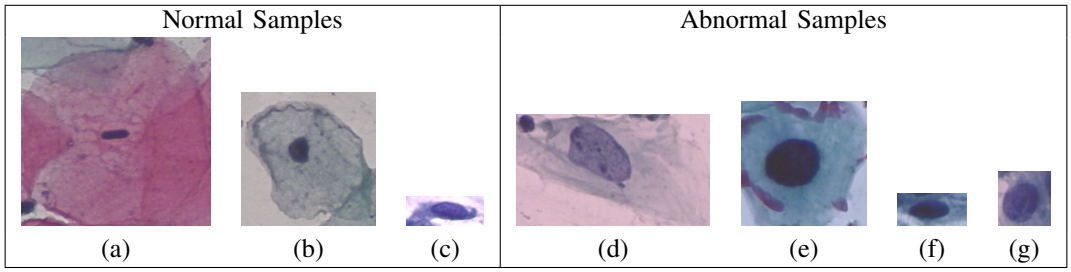

Fig. 1. Samples of the pap-smear dataset: Superficial squamous epithelial; (b) Intermediate squamous epithelial; (c) Columnar epithelial; (d) Mild squamous non-keratinizing dysplasia; (e) Moderate squamous non-keratinizing dysplasia; (f) Severe squamous non-keratinizing dysplasia; (g) Squamous cell carcinoma in situ intermediate [26].

C. Classifiers

After extracting the texture features, we used two different approaches to classify the samples into their respective classes. A brief description of the classifiers is given as follows:

- K-Nearest Neighbors (KNN): this classifier uses a comparison of instances and a voting scheme to classify the samples. For each input sample, KNN compares this sample with all training samples using a similarity metric and selects the K closest ones. Then, it attributes to the input sample the most common class among the K selected samples. For the experiments, we used as similarity metrics the Euclidean distance, $K = 1$, and standardized features;
- Linear Discriminant Analysis (LDA): this statistical classifier is based on Fisher's discriminant function [40]. This statistical method is grounded on Bayes' theorem and aims to find a linear combination of features in order to separate the classes. For this, it takes into account the average feature vector μ_i of each class, and the covariance matrix Σ of the features (Σ is the same for all the classes).
- Support Vector Machine (SVM): this classifier is based on statistical learning frameworks. Its main goal is to find a hyperplane in an N-dimensional space that best separates two sets of data points. It considers that the best hyperplane is the one that has the maximum margin, i.e., the maximum distance between data points of the two sets. In this work, we used LIBSVM [41] and its default parameter values.

To validate both classifiers we used *5-fold cross-validation*. We report the average accuracy among folds as also the standard deviation.

IV. Results and Discussion

Images in the pap-smear database present color information. To compute the texture features for each method we discarded this information and used the grayscale versions of the images obtained by using its luminance. For some texture methods, the number of features obtained depends on some parameters, eg., the number of box sizes used for the lacunarity methods or the dilation radius used in the Bouligand-Minkowski fractal dimension method. For these methods, we selected the configuration that resulted in the highest accuracy. We evaluated each method using both LDA and KNN classifiers and focused only on the two-class problem: normal and abnormal.

Table I shows the results obtained by each method. Each classifier achieved its best results using a different texture method: "RNN descriptor (rotation invariance)" for KNN (82.89), "Fractal (Bouligand-Minkowski)" for LDA (86.91), and "Tourist walk" for SVM (86.92). Oppositely, for all classifiers we obtain the worst result when we use the descriptors obtained by the "Lacunarity (local)" method: 69.03, 73.61, and 73.61 for, respectively, KNN, LDA, and SVM.

Except for Discrete Cosine Transform (DCT), all other methods present a better performance when using LDA or SVM as a classifier instead of the KNN. In general, LDA performs slightly better than SVM in most of the texture methods, with a result usually 2.59% better than SVM. Oppositely, when SVM surpasses LDA, it is usually only 1.06% better.

We also evaluated how the combination of different texture features could improve the classification accuracy of *pap-smear* images. Due to a large number of selected texture methods, it would be time-consuming to evaluate all 2^{19} possible combinations. Instead, we used Particle Swarm Optimization (PSO) [42] to select the best combination of methods. To accomplish that, we represented the selected methods as a particle at position $[X(1), X(2), \ldots, X(D)]$ in the search space, where $D = 19$ is the number of dimensions (texture methods). We considered that an i-th method must be included in the combination if $X(i) \geq 0.5$. For the measure of the quality of the selected combination, we considered the accuracy.

Table II shows the texture features selected by each classifier. As one can see, SVM selected more methods (12) while LDA selected less (9). In general, there is a little intersection among the selections performed by each classifier. Of the 19 methods available, only 4 of them are selected by all classifiers: "Lacunarity (global)", "Lacunarity (local)", "Lacunarity 3D" and "Fractal (Bouligand-Minkowski)". It is interesting to notice that they are all related to the complexity analysis of the image, indicating that this kind of feature may play an important role in the discrimination of the samples. The combination of features improves the accuracy for all classifiers: 7.19 % for KNN, 5.46 % for LDA, and 5.56 % for SVM. Although KNN presents the best improvement in accuracy, LDA and SVM still perform better than KNN.

TABLE I
SUCCESS RATE OBTAINED FOR EACH METHOD. METHOD MARKED WITH * MEANS THAT THE NUMBER OF FEATURES WAS DEFINED TO MAXIMIZE THE ACCURACY.

Method	# features	KNN	LDA	SVM
First order	5	75.90 ± 3.99	78.19 ± 2.13	78.19 ± 1.34
Fourier descriptors	15	70.12 ± 2.40	77.64 ± 2.30	73.83 ± 0.39
Wavelet descriptors	18	79.94 ± 2.51	86.48 ± 1.56	86.37 ± 1.59
Haralick	16	70.88 ± 2.19	79.94 ± 1.57	73.94 ± 0.52
DCT	8	81.35 ± 2.60	78.73 ± 1.58	80.81 ± 1.20
GLDM	60	76.88 ± 1.84	84.08 ± 2.80	85.17 ± 1.69
LBP ($R = 1$)	8	75.57 ± 3.21	80.05 ± 2.02	77.21 ± 1.61
LBP ($R = 2$)	16	77.32 ± 1.97	83.21 ± 1.26	83.53 ± 1.72
LBP ($R = 3$)	24	78.52 ± 3.32	82.01 ± 0.55	83.42 ± 0.60
Differential lacunarity	*	68.15 ± 3.10	76.34 ± 1.61	74.15 ± 0.83
Lacunarity (global)	*	69.68 ± 3.79	77.97 ± 1.32	73.61 ± 0.36
Lacunarity (local)	*	69.03 ± 2.03	73.61 ± 1.25	73.61 ± 0.36
Lacunarity 3D	*	73.39 ± 2.05	77.32 ± 0.72	74.15 ± 1.11
Fractal (average square difference)	*	73.83 ± 1.79	84.52 ± 1.16	80.37 ± 0.88
Fractal (Mass-radius)	*	79.83 ± 3.50	82.45 ± 1.97	84.19 ± 0.88
Fractal (Bouligand-Minkowski)	*	77.64 ± 2.65	86.91 ± 1.84	85.17 ± 1.47
LBP+FD	80	79.49 ± 4.10	83.97 ± 2.18	84.52 ± 0.88
Tourist walk	48	76.23 ± 1.47	85.61 ± 1.12	86.92 ± 0.99
RNN descriptor (rotation invariance)	30	82.89 ± 3.17	84.08 ± 1.69	83.97 ± 1.43

TABLE II
TEXTURE DESCRIPTORS SELECTED BY PSO ALGORITHM.

Method	KNN	LDA	SVM
First order		X	
Fourier descriptors		X	X
Wavelet descriptors	X		X
Haralick			
DCT	X		
GLDM		X	X
LBP ($R = 1$)	X		
LBP ($R = 2$)	X		X
LBP ($R = 3$)	X		
Differential lacunarity			X
Lacunarity (global)	X	X	X
Lacunarity (local)	X	X	X
Lacunarity 3D	X	X	X
Fractal (average square difference)		X	
Fractal (Mass-radius)	X		
Fractal (Bouligand-Minkowski)	X	X	X
LBP+FD			X
Tourist walk	X		X
RNN descriptor (rotation invariance)		X	X
Success rate	90.08 ± 1.18	92.37 ± 1.43	92.48 ± 2.59

Table III shows the accuracy of the combination of texture features selected by PSO and its comparison with other approaches addressing the same problem. Except for the work of [25], our approach was capable to surpass all compared methods by simply combining texture features obtained using traditional texture analysis methods. The approach proposed in [25] uses the features obtained by three Convolutional Neural Networks (Inception-v3, Resnet152 and Inception-Resnet-v2) pretrained on ImageNet [43]. This enables these CNNs to learn generic image features that can be used in a wide variety of image classification problems without training from scratch. Still, our approach proved to be competitive in terms of average success rate and standard deviation.

TABLE III
PERFORMANCE COMPARISON OF DIFFERENT METHODS ON *pap-smear* DATASET.

Method	Success rate
Inception-v3 with transfer learning [44]	89.66 ± 1.89
Resnet152 with transfer learning [44]	90.87 ± 1.48
Inception – Resnet v2 with transfer learning [44]	89.25 ± 2.23
Concatenation network [25]	92.63 ± 1.68
SIFT(BoW(VQ)+SPM+SVM) [45]	84.03 ± 2.30
LBP(BoW(VQ)+SPM+SVM) [45]	81.43 ± 2.10
SAHLBP(BoW(VQ)+SPM+SVM) [23]	86.21 ± 2.00
SIFT+SAHLBP(BoW(VQ)+SPM+SVM) [23]	87.63 ± 2.10
SIFT(BoW(LLC)+SPM+Softmax) [24]	89.96 ± 1.40
Proposed (PSO + KNN)	90.08 ± 1.18
Proposed (PSO + LDA)	92.37 ± 1.43
Proposed (PSO + SVM)	92.48 ± 2.59

V. CONCLUSION

In this paper, we addressed the problem of *pap-smear* image classification using texture features. We evaluated, independently, different texture features and their combination

using three different classifiers: KNN, LDA, and SVM. By combining the texture features, our approach obtained a high performance and surpassed most of the compared methods (LDA and SVM experiment), including some deep learning approaches. We believe that our proposed fused signature provides a relevant tool for the *pap-smear* classification task, and, therefore, adds a new tool to the computer vision research focused on the Papanicolaou test.

ACKNOWLEDGMENTS

André R. Backes gratefully acknowledges the financial support of CNPq (National Council for Scientific and Technological Development, Brazil) (Grant #307100/2021-9). This study was financed in part by the Coordenação de Aperfeiçoamento de Pessoal de Nível Superior - Brazil (CAPES) - Finance Code 001.

REFERENCES

[1] H. Xie, D. Yang, N. Sun, Z. Chen, and Y. Zhang, "Automated pulmonary nodule detection in CT images using deep convolutional neural networks," *Pattern Recognition*, vol. 85, pp. 109 – 119, 2019.

[2] D. M. Vo, N.-Q. Nguyen, and S.-W. Lee, "Classification of breast cancer histology images using incremental boosting convolution networks," *Information Sciences*, vol. 482, pp. 123 – 138, 2019.

[3] M. M. Abdelsamea, A. Pitiot, R. B. Grineviciute, J. Besusparis, A. Laurinavicius, and M. Ilyas, "A cascade-learning approach for automated segmentation of tumour epithelium in colorectal cancer," *Expert Systems with Applications*, vol. 118, pp. 539 – 552, 2019.

[4] A. R. Backes, A. S. Martinez, and O. M. Bruno, "Texture analysis based on maximum contrast walker," *Pattern Recognition Letters*, vol. 31, no. 12, pp. 1701 – 1707, 2010.

[5] L. M. Kaplan, "Extended fractal analysis for texture classification and segmentation," *IEEE Transactions on Image Processing*, vol. 8, no. 11, pp. 1572–1585, 1999.

[6] A. Humeau-Heurtier, "Texture feature extraction methods: A survey," *IEEE Access*, vol. 7, pp. 8975–9000, 2019.

[7] R. M. Haralick, "Statistical and structural approaches to texture," *Proceedings of the IEEE*, vol. 67, no. 5, pp. 786–804, 1979.

[8] J. Chen, S. Shan, C. He, G. Zhao, M. Pietikainen, X. Chen, and W. Gao, "WLD: A robust local image descriptor," *IEEE Transactions on Pattern Analysis and Machine Intelligence*, vol. 32, no. 9, pp. 1705–1720, 2010.

[9] R. Azencott, J.-P. Wang, and L. Younes, "Texture classification using windowed fourier filters," *IEEE Trans. Pattern Anal. Mach. Intell*, vol. 19, no. 2, pp. 148–153, 1997.

[10] B. S. Manjunath and W.-Y. Ma, "Texture features for browsing and retrieval of image data," *IEEE Trans. Pattern Anal. Mach. Intell*, vol. 18, no. 8, pp. 837–842, 1996.

[11] A. R. Backes, D. Casanova, and O. M. Bruno, "Texture analysis and classification: A complex network-based approach," *Information Sciences*, vol. 219, pp. 168–180, 2013.

[12] ——, "Color texture analysis based on fractal descriptors," *Pattern Recognition*, vol. 45, no. 5, pp. 1984–1992, 2012.

[13] J. J. M. Sá Junior, A. R. Backes, and P. C. Cortez, "Texture analysis and classification using shortest paths in graphs," *Pattern Recognition Letters*, vol. 34, no. 11, pp. 1314–1319, 2013.

[14] J. J. M. Sá Junior, P. C. Cortez, and A. R. Backes, "Color texture classification using shortest paths in graphs," *IEEE Transactions on Image Processing*, vol. 23, no. 9, pp. 3751–3761, 2014.

[15] V. Andrearczyk and P. F. Whelan, "Using filter banks in convolutional neural networks for texture classification," *Pattern Recognition Letters*, vol. 84, pp. 63 – 69, 2016.

[16] J. J. M. Sá Junior and A. R. Backes, "ELM based signature for texture classification," *Pattern Recognition*, vol. 51, pp. 395–401, 2016.

[17] J. J. Sá Junior, A. R. Backes, and O. M. Bruno, "Randomized neural network based signature for color texture classification," *Multidimensional Systems and Signal Processing*, Jun 2018, doi:10.1007/s11045-018-0600-6.

[18] M. Crosier and L. D. Griffin, "Using basic image features for texture classification," *International Journal of Computer Vision*, vol. 88, no. 3, pp. 447–460, 2010.

[19] P. Wang, L. Wang, Y. Li, Q. Song, S. Lv, and X. Hu, "Automatic cell nuclei segmentation and classification of cervical pap smear images," *Biomedical Signal Processing and Control*, vol. 48, pp. 93 – 103, 2019.

[20] A. Tareef, Y. Song, H. Huang, D. Feng, M. Chen, Y. Wang, and W. Cai, "Multi-pass fast watershed for accurate segmentation of overlapping cervical cells," *IEEE Transactions on Medical Imaging*, vol. 37, no. 9, pp. 2044–2059, 2018.

[21] Y. Liu, P. Zhang, Q. Song, A. Li, P. Zhang, and Z. Gui, "Automatic segmentation of cervical nuclei based on deep learning and a conditional random field," *IEEE Access*, vol. 6, pp. 53 709–53 721, 2018.

[22] K. Bora, M. Chowdhury, L. B. Mahanta, M. K. Kundu, and A. K. Das, "Automated classification of pap smear images to detect cervical dysplasia," *Computer Methods and Programs in Biomedicine*, vol. 138, pp. 31–47, 2017. [Online]. Available: https://www.sciencedirect.com/science/article/pii/S0169260716303583

[23] D. Liu, S. Wang, D. Huang, G. Deng, F. Zeng, and H. Chen, "Medical image classification using spatial adjacent histogram based on adaptive local binary patterns," *Computers in Biology and Medicine*, vol. 72, pp. 185–200, 2016. [Online]. Available: https://www.sciencedirect.com/science/article/pii/S0010482516300646

[24] D. Lin, Z. Lin, L. Sun, K.-A. Toh, and J. Cao, "Llc encoded bow features and softmax regression for microscopic image classification," in *2017 IEEE International Symposium on Circuits and Systems (ISCAS)*, 2017, pp. 1–4.

[25] L. D. Nguyen, D. Lin, Z. Lin, and J. Cao, "Deep cnns for microscopic image classification by exploiting transfer learning and feature concatenation," in *ISCAS*. IEEE, 2018, pp. 1–5.

[26] J. Jantzen, J. Norup, G. Dounias, and B. Bjerregaard, "Pap-smear benchmark data for pattern classification," in *Proc. NiSIS 2005*. NiSIS, 2005, pp. 1–9.

[27] R. M. Haralick, "Statistical and structural approaches to texture," *Proc. IEEE*, vol. 67, no. 5, pp. 768–804, 1979.

[28] I. Daubechies, *Ten lectures on wavelets*. Society for Industrial and Applied Mathematics, 1992.

[29] T. Chang and C.-C. Kuo, "Texture analysis and classification with tree-structure wavelet transform," *IEEE Transactions on Image Processing*, vol. 2, no. 4, pp. 429–441, 1993.

[30] J. S. Weszka, C. R. Dyer, and A. Rosenfeld, "A comparative study of texture measures for terrain classification," *IEEE Transactions on Systems, Man, and Cybernetics*, vol. 6, no. 4, pp. 269–285, 1976.

[31] I. Ng, T. Tan, and J. Kittler, "On local linear transform and Gabor filter representation of texture," in *International Conference on Pattern Recognition*, 1992, pp. 627–631.

[32] T. Ojala, M. Pietikainen, and T. Maenpaa, "Multiresolution gray-scale and rotation invariant texture classification with local binary patterns," *IEEE Trans. Pattern Analysis and Machine Intelligence*, vol. 24, no. 7, pp. 971–987, Jul. 2002.

[33] A. R. Backes, "A new approach to estimate lacunarity of texture images," *Pattern Recognition Letters*, vol. 34, no. 13, pp. 1455–1461, 2013.

[34] P. Dong, "Test of a new lacunarity estimation method for image texture analysis," *International Journal of Remote Sensing*, vol. 21, no. 17, pp. 3369–3373, 2000.

[35] A. R. Backes and J. J. M. Sá Junior, "Texture classification using fractal dimension improved by local binary patterns," in *European Signal Processing Conference - EUSIPCO*. IEEE, 2018, pp. 1312–1316.

[36] A. R. Backes, W. N. Gonçalves, A. S. Martinez, and O. M. Bruno, "Texture analysis and classification using deterministic tourist walk," *Pattern Recognition*, vol. 43, no. 3, pp. 685–694, 2010.

[37] A. R. Backes, "Upper and lower volumetric fractal descriptors for texture classification," *Pattern Recognition Letters*, vol. 92, pp. 9–16, 2017.

[38] G. Landini and J. W. Rippin, "Notes on the implementation of the mass-radius method of fractal dimension estimation," *Comput. Appl. Biosci*, vol. 9, no. 5, pp. 547–550, 1993.

[39] M. Petrou and P. GarcSevilla, *Image processing - dealing with texture.* Wiley, 2006.

[40] R. A. Fisher, "The use of multiple measurements in taxonomic problems," *Annals of Eugenics*, vol. 7, no. 7, pp. 179–188, 1936.

[41] C.-C. Chang and C.-J. Lin, "LIBSVM: A library for support vector machines," *ACM Transactions on Intelligent Systems and Technology*, vol. 2, pp. 27:1–27:27, 2011. [Online]. Available: http://www.csie.ntu.edu.tw/~cjlin/libsvm

[42] J. Kennedy and R. Eberhart, "Particle swarm optimization," in *Proceedings of ICNN'95 - International Conference on Neural Networks*, vol. 4, 1995, pp. 1942–1948 vol.4.

[43] J. Deng, W. Dong, R. Socher, L. J. Li, K. Li, and L. F. Fei, "Imagenet: A large-scale hierarchical image database," in *CVPR*, 2009, pp. 248–255. [Online]. Available: http://dx.doi.org/10.1109/CVPRW.2009.5206848

[44] G. J. Scott, M. R. England, W. A. Starms, R. A. Marcum, and C. H. Davis, "Training deep convolutional neural networks for land-cover classification of high-resolution imagery," *IEEE Geosci. Remote. Sens. Lett*, vol. 14, no. 4, pp. 549–553, 2017.

[45] S. Lazebnik, C. Schmid, and J. Ponce, "Beyond bags of features: Spatial pyramid matching for recognizing natural scene categories," in *2006 IEEE Computer Society Conference on Computer Vision and Pattern Recognition (CVPR'06)*, vol. 2, 2006, pp. 2169–2178.